Self-Deformable Flexible MEMS Tweezer Composed of Poly(Vinylidene Fluoride)/Ionic Liquid Gel for Electrical Measurements and Soft Gripping

Takafumi Yamaguchi, *Graduate Student Member, IEEE*, Naoto Usami, *Member, IEEE*, Kei Misumi, *Graduate Student Member, IEEE*, Atsushi Toyokura, Akio Higo, *Member, IEEE*, Shimpei Ono, Gilgueng Hwang, *Member, IEEE*, Guilhem Larrieu, *Member, IEEE*, Yoshiho Ikeuchi, Agnés Tixier-Mita, *Member, IEEE*, Ken Saito, *Member, IEEE*, Timothée Lévi, *Member, IEEE*, and Yoshio Mita, *Senior Member, IEEE*

***Abstract*— We present a self-deformable flexible tweezer capable of simultaneous mechanical handling and electrical measurements. The tweezer has a soft cantilever with the dimensions 2 mm × 8 mm × 75-100 μm, and undergoes self-deformation. The device is shown to be successfully capable of detecting electrical signals by gently touching the surface and grasping a spherical bead. The device demonstrated the lowest working voltage (1.5 V_{DC}), force suitable for soft gripping, and curvature radius of 2 mm, that was one of the smallest values compared to that of similar state-of-the-art devices. The device was fabricated using a unique and highly reliable process that was specifically developed to produce flexible cantilevers with novel ionic polymer-metal composites (IPMCs). The materials used were poly(vinylidene fluoride-co-trifluoroethylene) (PVDF-TrFE) and an ionic liquid (IL). The PVDF-TrFE/IL gel was prepared using acetone as the solvent and the gel was coated with silver nanowires as the electrodes. The actuator with a length of 8 mm and containing 50 wt% IL yielded the largest bending displacement of 7 mm and minimum curvature radius of 2 mm at 1.5 V_{DC}. [2022-0026]**

***Index Terms*— Electrical detection, flexible actuator, ionic liquid, PVDF-TrFE, self-deformable cantilever, silver nanowire, soft gripping.**

Manuscript received 28 February 2022; revised 5 May 2022; accepted 23 May 2022. Date of publication 29 July 2022; date of current version 3 October 2022. This work was supported in part by the Core Research for Evolutional Science and Technology (CREST) under Grant Japan Science and Technology Agency (JST) JPMJCR20T2 and in part by the Internal Project of the Laboratory for Integrated Micro Mechatronic Systems (LIMMS), National Center for Scientific Research (CNRS)-The University of Tokyo (UTokyo) Institute of Industrial Science (IIS), Unité Mixte Initernationale (UMI) 2080. Subject Editor H. Fujita. *(Corresponding author: Yoshio Mita.)*

Takafumi Yamaguchi, Kei Misumi, Atsushi Toyokura, and Akio Higo are with the Department of Electrical Engineering and Information Systems, The University of Tokyo (UTokyo), Tokyo 113-8656, Japan.

Naoto Usami is with the Institute of Space and Astronautical Science (ISAS), Japan Aerospace Exploration Agency (JAXA), Chuo-ku, Sagamihara, Kanagawa 252-5210, Japan.

Shimpei Ono is with the Central Research Institute of Electric Power Industry, Yokosuka, Kanagawa 240-0196, Japan.

Gilgueng Hwang is with the Laboratory for Integrated Micro Mechatronic Systems (LIMMS), National Center for Scientific Research (CNRS), UTokyo, Tokyo 153-8505, Japan, and also with C2N-CNRS, Paris-Saclay University, 91120 Palaiseau, France.

Guilhem Larrieu is with the Laboratory for Integrated Micro Mechatronic Systems (LIMMS), National Center for Scientific Research (CNRS), UTokyo, Tokyo 153-8505, Japan, and also with LAAS-CNRS, 31400 Toulouse, France.

Yoshiho Ikeuchi is with the Laboratory for Integrated Micro Mechatronic Systems (LIMMS), National Center for Scientific Research (CNRS), UTokyo, Tokyo 153-8505, Japan, and also with the Institute of Industrial Science, UTokyo, Tokyo 153-8905, Japan.

Agnés Tixier-Mita is with the Laboratory for Integrated Micro Mechatronic Systems (LIMMS), National Center for Scientific Research (CNRS), UTokyo, Tokyo 153-8505, Japan, and also with the Research Center for Advanced Science and Technology, UTokyo, Tokyo 153-8904, Japan.

Ken Saito is with the Department of Precision Machinery Engineering, Nihon University, Chiba 274-8501, Japan.

Timothée Lévi is with the Laboratory for Integrated Micro Mechatronic Systems (LIMMS), National Center for Scientific Research (CNRS), UTokyo, Tokyo 153-8505, Japan, and also with IMS-CNRS, University of Bordeaux, 33000 Bordeaux, France.

Yoshio Mita is with the Department of Electrical Engineering and Information Systems, The University of Tokyo (UTokyo), Tokyo 113-8656, Japan, and also with the Laboratory for Integrated Micro Mechatronic Systems (LIMMS), National Center for Scientific Research (CNRS), UTokyo, Tokyo 153-8505, Japan (e-mail: mems@if.t.u-tokyo.ac.jp).

This article has supplementary material provided by the authors and color versions of one or more figures available at https://doi.org/10.1109/JMEMS.2022.3187428.

Digital Object Identifier 10.1109/JMEMS.2022.3187428

I. Introduction

MICROGRIPPERS are expected to be the next-generation devices for various applications such as manipulation, assembly, or pick-and-place tasks by grabbing the microobjects [1]. Different methods of their actuations have been studied such as piezoelectric [2]–[4], electrostatic [5], [6], electrothermal [4], [7], [8] and ionic polymer-metal composite (IPMC) [9]–[12] actuators. Jain *et al.* (2014) [2] designed the three degree-of-freedom-based microgripper with piezoelectric actuator for microassembly. It involved conducting sequential pick-and-place of a micro pin in a hole driven by robust control of the applied voltage. Jaiswal *et al.* (2017) [3] fabricated the piezoelectric microtweezer with the flexible SU-8 end effector to measure the stiffness of spherical cells. Its force sensing by optical observation of the deflection of the actuator enables wide measurement of the forces ranging from less than one hundred nN to one mN. The main advantages of the piezoelectric grippers are small displacement

of micro/nano scale, fast response of micro/nano-range second, precise control, and large gripping force [2]. The electrostatic actuator integrated in the microgrippers is also driven by voltage as a comb-drive mechanism. The electrostatic grippers sometimes grab soft materials such as a polystyrene sphere (Chen *et al.* (2009) [5]) or lilium pollen (Piriyanont and Moheimani (2015) [6]). To avoid the damage to the targets, the former electrostatic microtweezer has the piezoresistive sensors on the side wall of the actuator and the latter microgripper has electrothermal force sensors with the feedback control. The electrostatic microgrippers have advantages that the sensors are easily integrated in the grippers with microelectromechanical system (MEMS) technology, they are capable of grasping objects from a wide dimension range in μm scale, and they are operated stably even in ambient or vacuum environments [5]. The electrothermal microgrippers are often used to manipulate soft materials because of their flexibility, large deformation, strong recovery force, low operating voltage, and compact structure [7]. Zhang *et al.* (2012) [7] designed the electrothermal SU-8 microgripper with a jaw for a large gripping scope. This gripper grasps the biological objects of different sizes such as a micro blood vessel and cyanobacteria cells for micromanipulation. The electrothermal microgripper is also integrated with the piezoresistive built-in force sensor in its jaw to firmly hold objects such as a glass sphere (Duc *et al.* (2008) [8]). Moreover, Rakotondrabe and Ivan (2011) [4] designed the microgripper composed of an actuator operated by electrothermal and piezoelectric effects for micropositioning. It works as a combination of the thermal actuation (coarse positioning) and piezoelectric effect (fine positioning), demonstrating the high range and resolution of a pick-and-place task of a polystyrene sphere. Finally, IPMC is a voltage-driven electroactive polymer, which has recently drawn attraction mainly for its high flexibility and large deformation at low operating voltage [9]. The handling targets of the IPMC tweezers are of various sizes and stiffness such as micropin [10], nut and ping-pong ball [9], fish egg [11], hydrogel and solder ball [12]. The IPMC microgripper is suitable for both industrial operations and bio-micromanipulation tasks [12].

As discussed above, various targets from hard metal pins and plastic spheres to vulnerable organisms are manipulated by the microgripper actuated by different mechanisms [2]–[12]. It is necessary to analyze the gripped objects in the industrial, material, and biological manipulation, especially fragile materials with unknown characteristics, because simultaneous manipulation and observation allows for more efficient verification of their electrical properties. Therefore, the microtweezer should grip a vulnerable target slowly and gently, not give unnecessary stimuli, and observe it electrically with close contact. Our attempts to observe a three-dimensional (3D) delicate object while it is gripped led us to propose an active flexible tweezer device, as shown in Fig. 1. This device, equipped with a self-deformable flexible cantilever, is capable of gripping a 3D target of even spherical structures with minimum force to closely perform adequate electrical measurements. An example of the proposed tweezer demonstrating gripping and electrical observation is an

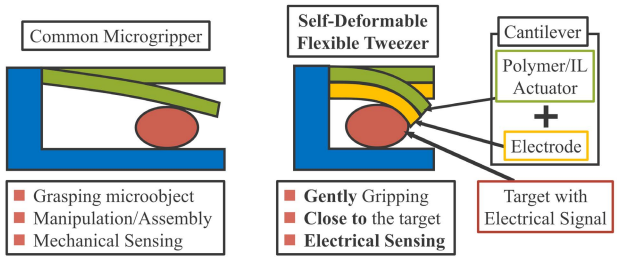

Fig. 1. Common microgripper for micromanipulation and self-deformable close tweezer gripping of a target to detect an electrical signal.

organism [1]. Microelectrode array-type two-dimensional (2D) devices are commonly used to detect electrical responses from organisms [13], [14]. However, a major disadvantage of these devices is their planar structure, that is, their inability to adhere to cellular tissues of the organisms, which are essentially 3D structures. Moreover, owing to their passivity, these devices can only detect the response from those parts of organism which are in their contact. Our active flexible tweezer can overcome these problems because the device can fix gently and adhere closely to the spherical organism and non-invasively measure electrical signals from the target.

The flexible cantilever of the tweezer in Fig. 1 was realized based on an IPMC actuator. Our suggested use of this actuator was motivated by its excellent suitability as an active device for gripping vulnerable objects as a result of its high flexibility, biocompatibility, huge strain, good conductivity, and low operating voltage without heating compared with other actuators [9]. An IPMC actuator is composed of polymers and mobile ions (cations and anions) and is equipped with electrodes. Theories that have been proposed to explain the deformation of IPMCs when voltage is applied are based on the size difference [15], the diffusion speed of ions [16], or the one-directional movement of ions [17]. In all these studies, the actuators deflected to one side when voltage was applied. The polymer is the main component of an IPMC actuator and various polymers, such as Nafion [9]–[12] or poly(vinylidene fluoride) (PVDF) [15], [18], have been used in this regard. IPMC actuators based on PVDF or its co-polymers and ionic liquids (ILs) as the source of mobile ions have a large strain of a few % at operating voltages below 10 V [15], [18]–[22]. PVDF and its co-polymers are ferroelectric and piezoelectric materials with a low Young's modulus (~500 MPa) [21]. Ionic liquids are salts that maintain their fluid state across a wide range of temperatures and are characterized by low vapor pressure, incombustibility, and good conductivity [15]. Among the IPMCs configured with PVDF co-polymers and an IL, the IPMC actuator (composed of poly(vinylidene fluoride-co-trifluoroethylene) (PVDF-TrFE) and 1-ethyl-3-methylimidazolium bis(trifluoromethanesulfonyl)imide (EMIMTFSI) as the IL) is known to have the largest displacement of 3.5 mm for an actuator length of 10 mm at 100 mHz and 5.0 V_{pp} [21].

These advantages prompted our decision to base the actuator on PVDF-TrFE/EMIMTFSI ionic gel composites with the ultimate aim of realizing a self-deformable flexible tweezer

capable of gripping a target gently to measure its electrical characteristics (Fig. 1). The electrode of the designed actuator consists of an assembly of silver nanowires (AgNWs) using acetone as the solvent. This assembly of nm-scale silver wires has higher flexibility and conductivity than sheet-form metal electrodes. The combination of the PVDF-TrFE/EMIMTFSI gel with AgNWs using acetone as the solvent is unique and has, to the best of our knowledge, only been used by us [1]. Particularly, we previously reported an actuator based on this novel "ionic gel." This actuator delivered a displacement of 7 mm, which was 88 % of the total length of the actuator, at 1.5 V (V_{DC}) [1]. This actuator had one of the highest normalized strains among state-of-the-art IPMC actuators at the lowest operating voltage. The tweezer fabricated with this ionic gel actuator could also detect electrical signals in contact with the Au target electrode. However, the actuator had two major drawbacks: a low manufacturing yield of 33 % and low deformation speed of 2.3 mm/min. Moreover, although the actuator succeeded in detecting an electrical signal, we were unable to demonstrate that the tweezer performed the manipulation and gripping action satisfactorily.

In this study, we developed a new fabrication process for our ionic gel using the same materials from the previous actuator to improve its production yield and deformation properties. The new ionic gel has deformation properties superior to those of the former gel under the same electrical conditions. The latest actuator was similarly mounted on a tweezer device to detect electrical signals and to perform the grasping motion. The generated force of the actuator was estimated when the tweezer was gripping the target. Consequently, the tweezer with our PVDF-TrFE/EMIMTFSI gel actuator with the AgNWs electrode as the cantilever was confirmed to be capable of gripping the spherical target and detecting electrode signals for manipulating 3D targets such as organisms and detecting their signals.

II. Fabrication of Ionic Gel Tweezer

A. Materials

The ionic liquid, EMIMTFSI, with a purity of 98.0 %, was purchased from the Tokyo Chemical Industry (Japan) and was stored and used in a glove box under a nitrogen atmosphere. The co-polymer, PVDF-TrFE (PIEZOTECH® FC25), contained 25 mol% trifluoroethylene (TrFE) and was obtained from Arkema Piezotech (France). For the solvent, we used acetone with a purity of 99.5 % obtained from Kanto Chemical Holdings (Japan). The PVDF-TrFE and acetone were maintained at 25 % humidity in an atmospheric environment. The electrode was fabricated using an aqueous suspension of 5 mg/mL silver nanowires (AgNWs), purchased from Merck (Germany). The suspension was maintained at atmospheric pressure in the refrigerator (2-6 °C).

B. Fabrication of PVDF-TrFE/EMIMTFSI Ionic Gel Composites

Three PVDF-TrFE/EMIMTFSI ionic gel membranes were prepared by changing the weight ratio of PVDF-TrFE as 30, 50, and 70 wt% of the total weight of the ionic gel. The weight of PVDF-TrFE was 150 mg or 300 mg. Therefore, six ionic gel membranes were fabricated and denoted 30a, 30b, 50a, 50b, 70a, and 70b, where "30," "50," and "70" indicates the weight ratio of PVDF-TrFE/EMIMTFSI, and "a" and "b" indicate 150 mg or 300 mg PVDF-TrFE, respectively.

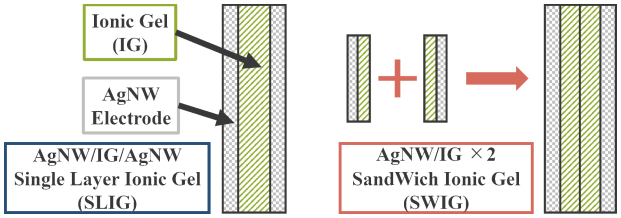

Fig. 2. Cross-sectional structure of the single-layer ionic gel (SLIG) and sandwich ionic gel (SWIG) membranes.

The ionic gel was fabricated as follows: 150 or 300 mg PVDF-TrFE powder was placed in a glass bottle with acetone and 5 wt% of the polymer solution. This solution was magnetically stirred on a hotplate at 50 °C for approximately 24 h. After stirring, an appropriate quantity of EMIMTFSI was added to the liquid. The PVDF-TrFE/EMIMTFSI in acetone was agitated at 50 °C for 24 h. This solution was spread in a Petri dish of ϕ 80 mm × 17 mm with a BEMCOT® lid, and dried at room temperature (25 °C) for 24 h to allow the acetone to evaporate.

The aforementioned procedure yielded four of the six ionic gel membranes (30b, 50a, 50b, and 70b). The other two films (30a and 70a) were destroyed owing to their thinness when peeled from the dish. The four membranes were coated with AgNWs to form the electrode.

C. Coating of Silver Nanowire Electrode

The electrode of the actuator consisted of a coating of AgNWs. We developed two methods to form the electrode: "single-layer ionic gel (SLIG)" and "sandwich ionic gel (SWIG)." A coating of AgNWs was applied to the 30b, 50a, 50b, and 70b films to form the SLIG, and only 50b was used to form the SWIG. First, a syringe was used to drop an aqueous suspension of AgNWs on one side of the ionic gel membranes in the Petri dish. This film was heated on a hotplate at 100 °C for 15 min and allowed to cool at 25 °C for 5 min. The SLIG was formed by peeling off the membrane coated with the electrode, after which the membrane was turned over to apply a coating of AgNWs on the other side of the ionic gel to form the second electrode. The film was dried as before to produce the SLIG membrane, and a cross-sectional view thereof is shown in Fig. 2 on the left. The SWIG membrane was obtained by attaching two films coated with AgNWs on one side via their ionic gel surfaces, as shown in Fig. 2 on the right, followed by heating at 100 °C on the hotplate for 10 min.

The composite film comprising the polymer/IL with electrodes was cut into a rectangular form of 2 mm × 10 mm using a UV laser cutter (LPKF Protolaser U4). The thickness of the SLIG before and after placement of the electrodes was measured using an Olympus LEXT OLS5000 laser microscope. The thicknesses of the 30b, 50a, 50b, and 70b actuators after applying the coating to form the electrodes were 52.6,

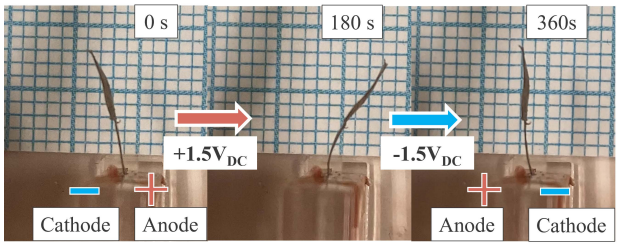

Fig. 3. Bidirectional bending motion of 50b SLIG actuator at ±1.5 V_{DC}.

65.6, 75.3, and 87.7 μm, respectively. The 50b SWIG with the electrodes was measured to have an approximate thickness of 100 μm by using a HITACHI Regulus 8230 scanning electron microscope.

D. Measurement Equipment

The electrical equipment used for measuring the characteristics of the ionic gel and tweezer are detailed in this section. In Subsection III-A and III-F (the characteristics of the actuator), a Hewlett-Packard E3640A was used as the DC power supply and the movement of the actuator was recorded by an iPhone camera. In Subsection III-D (the electrical measurements of the tweezer), a RIGOL DG4202 function generator, a HIOKI DT4253 (a digital multimeter) ammeter, a 1.5 V alkaline battery DC power supply, and a GWinstek GDS-2072A oscilloscope were used. The function generator produces an AC signal with 700 mV sinusoidal wave of 1 kHz. The capacitor and inductor settings were 10 pF and 47 mH, respectively. The math mode of the oscilloscope was used to analyze the V_{AC} signal. In this mode, the voltage at a particular frequency from the observed voltage can be detected using fast Fourier transformation. Finally in Subsection III-E (the gripping demonstration of the tweezer), the V_{DC} used was a ±1.5 V square wave from the function generator (RIGOL DG4202). The motion of the tweezer in Subsection III-D and III-E was recorded using an iPhone camera and a SONY HDR-PJ680 video camera.

III. Results and Discussion

A. Measurement of Deformation Characteristics in Ionic Gel Actuator

A 2 mm × 2 mm section of the 2 mm × 10 mm SLIG and SWIG actuators was fixed between a jig of copper tape electrodes. Then, DC power, V_{DC} was supplied to the actuator in the forward and reverse directions for 3 min to observe its bending motion. For the SLIG, the applied voltage was changed from 0.5-3.0 V_{DC} in increments of 0.5 V_{DC}. For the SWIG, the voltage was fixed at 1.5 V_{DC}. The displacement was measured in units of 1 mm using the graph sheet.

1) Deformation Properties of SLIG: The SLIG actuator always bent to the anode side, which was positively charged, as shown in Fig. 3 [1]. This was because the cations in IPMCs based on EMIMTFSI diffused faster than the anions [16]. All four actuators detected electrical signals at their maximum voltages owing to the destruction of the electric double layer in the ionic gel. During conduction, the current across the actuator suddenly increased to 3 A, which is the limit of the voltage supply. We observed that membranes 30b and 70b hardly deformed regardless of the direction of the applied voltage, although 50a and 50b exhibited significant deformation [1]. Except for the voltage levels at which the actuators conducted electricity, 50b exhibited the largest displacement of 7 mm at +1.5 V_{DC} and 5 mm at −1.5 V_{DC}, in Fig. 3 [1].

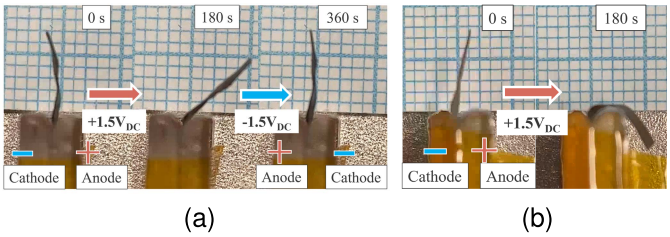

Fig. 4. Measurement of the deformation of the SWIG actuator. (a) Bidirectional bending motion of 50b at ±1.5 V_{DC}. Its estimated curvature radius was 5.29 mm by (1). (b) Deformation to the physical limit at the curvature radius of 2 mm. In both figures, the size of the smallest square on the graph paper is 1 mm × 1 mm.

TABLE I
PERFORMANCE COMPARISON OF SINGLE-LAYER IONIC GEL WITH SANDWICH IONIC GEL ACTUATOR

	SLIG	SWIG
PVDF-TrFE : IL weight content (mg)	300:300	300:300
Max. displacement (mm)	7	7
(Min.) working voltage (V)	1.5	1.5
Max. deforming speed (mm/min)	2.3	10.5
Yield (%)	33(5/15)	89(25/28)

2) Deformation Properties of SWIG: The 50b SWIG actuator was displaced by 7 mm at +1.5 V_{DC} and 6 mm at −1.5 V_{DC} in the direction of the anode, similar to the SLIG (Fig. 4(a)). Moreover, the 50b SWIG could undergo deformation almost to the physical limit of the minimum 2 mm curvature radius for a total length of 8 mm at 1.5 V_{DC} (Fig. 4(b)).

B. Performance Comparison of SLIG and SWIG

We compare the properties of 50b SLIG and 50b SWIG in Table I. In total, 15 SLIG of 50b and 28 SWIG of 50b were manufactured for validation of their yields. Both actuators underwent a maximum displacement of 7 mm at 1.5 V_{DC} working voltage for a PVDF-TrFE:EMIMTFSI weight content ratio of 300:300 mg (50b ionic gel). Meanwhile, SWIG outperformed SLIG with its maximum deformation speed 4.6 times as high and its yield 2.7 times as high as those of SLIG. The reason for the superior performance of SWIG compared with SLIG is the difference in the unevenness of the electrode coating. During the AgNW coating process of SLIG, the membrane with the electrode coating on one side was turned over to apply the AgNW coating to the reverse side. Membrane films coated with AgNWs on the reverse side shrink and contain many wrinkles because of the surface tension of the water in which the AgNWs are suspended and the internal stress resulting from the difference in Young's modulus between the ionic gel and AgNWs. Therefore, the electrode is printed unevenly on the reverse side such that the electrical conductivity of the electrodes is considered to

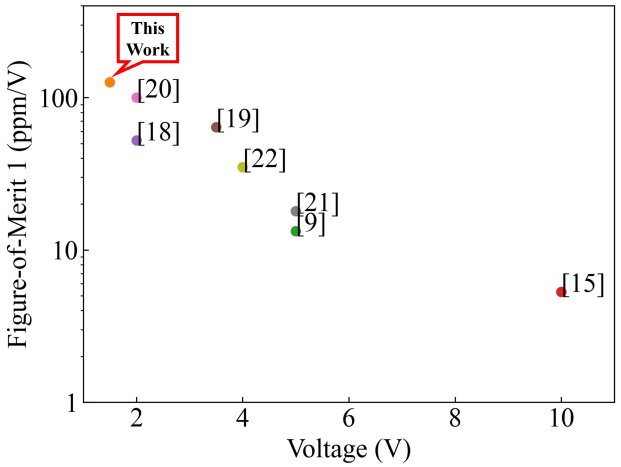

Fig. 5. Performance comparison in displacement by FoM_1.

be strongly influenced. However, the SWIG was fabricated by attaching the two membranes, each with an electrode coating on one side. This implies that the electrodes on both sides of the SWIG membrane were more uniform than those on SLIG because the SWIG membrane was not crumpled much by applying the electrode coating to only one side. As a result, SWIG would have higher electrical conductivity on the electrodes than SLIG, explaining the higher moving speed and yield of the former.

C. Performance Comparison of State-of-the-Art IPMCs

The 50b SWIG actuator with the largest 7 mm displacement and smallest 2.0 mm curvature radius at 1.5 V_{DC} was compared with the state-of-the-art IPMCs actuators produced from Nafion [9] or PVDF co-polymers [15], [18]–[22]. To appropriately evaluate the deformation, we employed the following equation, which is commonly used to compare the displacement of IPMC actuators [1], [9], [15], [18], [20], [21], [23].

$$\epsilon = \frac{2T\delta}{L^2 + \delta^2} (= \frac{T}{R}) \tag{1}$$

where ϵ, T, δ, L, and R are the normalized strain, thickness, displacement, deformed length projected on the unbent state, and curvature radius of the actuator, respectively. L is equal to the free length of the actuator when δ is sufficiently small compared to R. Now, ϵ is proportional to the working voltage V_{DC} in consideration of the deformation principle. Therefore, in this study, the next figure-of-merit (FoM_1) was defined for the evaluation.

$$FoM_1 = \frac{\epsilon}{V_{DC}} = \frac{T}{RV_{DC}} \tag{2}$$

The largest values of ϵ and δ in these studies are cited. The values in Table II and Fig. 5 indicate that our ionic gel actuator had the largest FoM_1 at the minimum working voltage of 1.5 V_{DC}. This huge FoM_1 was a consequence of the combination of PVDF-TrFE and EMIMTFSI. This combination has the largest displacement of PVDF co-polymer IPMC actuators [21], and the electrode with the AgNWs offers higher flexibility than metal electrodes in sheet form.

TABLE II
PERFORMANCE COMPARISON IN DISPLACEMENT BY FoM_1

Ref.	Material	T (μm)	V_{DC} (V)	R (mm)	ϵ (%)	FoM_1: ϵ/V_{DC} (ppm/V)
This Work	PVDF-TrFE	100	**1.5**	**5.29 (2.0)**	1.89	**126**
[9]	Nafion	300	5	45.0	0.666	13.3
[15]	PVDF	75	10	14.2	0.53	5.3
[18]	PVDF	150-175	2	14.3-16.7	1.05	52.5
[19]	PVDF-HFP	280	3.5	12.5	**2.24**	64.0
[20]	PVDF-HFP	106-162	2	5.3-8.1	2.0	100
[21]	PVDF-TrFE	50	5	5.56	0.899	18.0
[22]	PVDF-CTFE	**31-33**	4	**2.22**	1.40	34.9

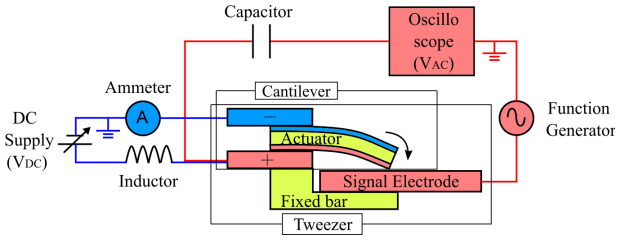

Fig. 6. Circuit of the tweezer device [1].

D. Demonstration of Tweezer as Electrical Probe

We demonstrated the tweezer illustrated in Fig. 6 by using our self-deformable ionic gel actuator as an electrical probe. Previously, we used 50b SLIG as probe of the tweezer [1]. However, in this study, a 50b SWIG was applied for the probe to detect the electrical signal because the SWIG has superior properties than SLIG. The cantilever of the actuator was held in place between the jig, which was the fixed electrode supplying power to the actuator of the printed circuits. The jig was composed of two electrodes for operation: the negative electrode was a fixed bar supplied with DC and the positive electrode was connected to the AC supply and was equipped with a Cu signal electrode. The blue circuit was powered by applying DC to operate the cantilever, whereas AC was supplied to the red circuit. The circuits were electrically separated by a capacitor and an inductor. When V_{DC} was applied to the electrodes in the DC circuit, the cantilever was deformed until it made contact with the Cu signal electrode ("+1.5 V_{DC}" applied situation and electrically "OFF" state of AC circuit). Because the red AC circuit conducted electricity as a result of the cantilever movement, V_{AC} was recorded by the oscilloscope ("+1.5 V_{DC}" applied and "ON"). After the connection of the probe and electrode, the reverse V_{DC} was applied so that the cantilever was operated to the opposite direction ("−1.5 V_{DC}" applied and "ON"). The AC circuit became open when the cantilever lost contact with the signal electrode ("−1.5 V_{DC}" applied and "OFF"). The cantilever repeatedly made contact with and was released from the signal electrode six times consecutively, as shown in Fig. 7. The V_{AC} level was recorded six times for repetition of the electrical ON and OFF state of the AC circuit and the readings were

TABLE III

AVERAGED V_{AC} FOR SIX TIMES OBSERVED AT 1 kHz BY THE TWEEZER BASED ON SLIG AND SWIG [1]

	Released Voltage	Contact Voltage
SLIG	43 mV	105 mV
SWIG	0.55 mV	14 mV

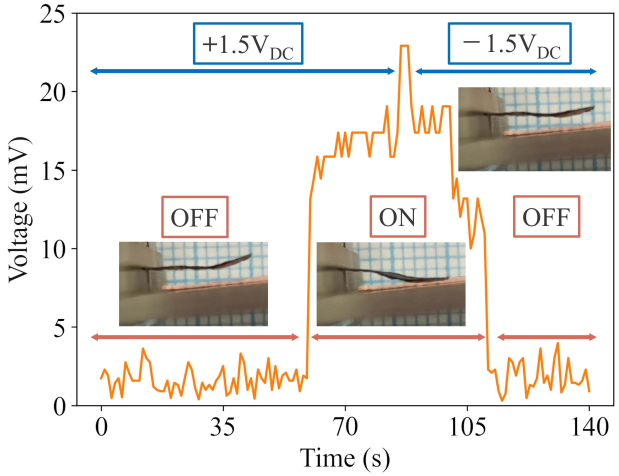

Fig. 7. Characteristics of the tweezer as the probe based on SWIG. ON/OFF movement of the tweezer and V_{AC} observed, during the third operation upon application of ±1.5 V_{DC}.

averaged. The change in the V_{AC} was recorded using a video camera.

Fig. 7 shows variation of the movement and voltage in the third instance of the repetition. In Fig. 7, the voltage was 0.5-3 mV from 0-60 seconds, when the cantilever was released from the signal electrode in the left "OFF" state of Fig. 7. From 60 to 85 seconds, the voltage suddenly increased to 13–17 mV, when the cantilever fully contacted the signal electrode in the middle electrical "ON" state. For 85–88 seconds, the voltage increased to 22 mV, because the DC circuit to move the cantilever (blue circuit in Fig. 6) became open for the change of the DC voltage from +1.5 V to −1.5 V and the AC current leaking through the inductor was supposed to flow into the red AC circuit. During 89–110 seconds, the voltage was 10–19 mV when the cantilever is "ON" state. However, the voltage was gradually decreasing during 100–110 seconds, because a part of the cantilever was leaving the electrode, as seen during 5–6 seconds of the supplementary movie. After 110 seconds, the voltage decreased greatly to 0.3–4 mV. This variation of the voltage means that the AC circuit became "OFF" when the cantilever was completely released from the electrode in Fig. 7. The results in Table III indicate that the observed signal voltage at 1 kHz averaged for six times at the time during which the cantilever was in contact with the Cu electrode ("ON" state) was more than 25 times as high as one when the cantilever was not making contact with the electrode ("OFF" state). These results confirmed that the cantilever based on our PVDF-TrFE/EMIMTFSI gel with an AgNW actuator was able to detect V_{AC} by making contact with and released from the signal electrode for the detection of the signal. The contact voltage of 14 mV in

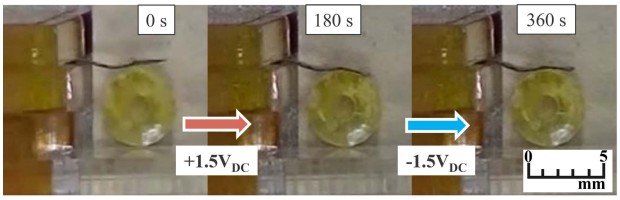

Fig. 8. Grasping motion of the tweezer based on SWIG with a 5 mm bead representing an organism.

the SWIG cantilever was approximately 10 times smaller than that in SLIG [1]. This is caused by the large surface resistance of AgNW electrode. The electrode resistance of the SLIG cantilever was calculated as approximately 500 kΩ [1]. However, the electrode resistance of the SWIG was measured by the digital multimeter as 7 MΩ, more than 10 times greater than that of SLIG. The AgNW electrode in SWIG is thought to deteriorate and lose conductivity due to reaction with ionic liquid or atmosphere during huge deformation.

E. Demonstration of the Gripping Function of the Tweezer

We demonstrated the gripping function of the tweezer. The tweezer was composed of a 50b SWIG actuator, jig fixing actuator, and an immobile bar, as shown in Fig. 8. The jig was composed of an acrylic plate with a thickness of 3 mm and copper tape electrodes. As described in Subsection III-A, an area sized 2 mm × 2 mm of the 2 mm × 10 mm SWIG was fastened between the copper electrodes. The grasping target was a plastic sphere with a diameter of 5 mm to imitate an organism. Application of ±1.5 V_{DC} for 3 min resulted in the actuator making repeated contact with and then releasing the target sphere, as shown in Fig. 8. These experiments confirmed that the tweezer with our ionic gel was able to grip the bead imitating an organism.

F. Measurement of Gripping Force and Young's Modulus of the SWIG Actuator

The gripping force of the tweezer during the grasping motion and Young's modulus of the cantilever of the tweezer were assessed by measurement of the structural values of the 50b SWIG actuator. In this study, this was accomplished by developing a simple method using the formula for the deformation of the cantilever, thereby obviating the need for the use of measuring equipment, such as a force sensor.

1) Estimation of the Gripping Force of the Tweezer: The actuator was operated as a cantilever, as described in Subsection III-A. The tip of the cantilever of the actuator was set to touch one of the overhead projector (OHP) film, as shown in Fig. 9. When 1.5 V_{DC} was applied to the electrode, the measuring cantilever imposed strain because the actuator underwent deformation to push the cantilever. This displacement was considered to be generated by the concentrated load at the free end as the pushing force of the actuator. Consequently, the displacement of the cantilever is given by (3):

$$d = \frac{wl^3}{3EI} \tag{3}$$

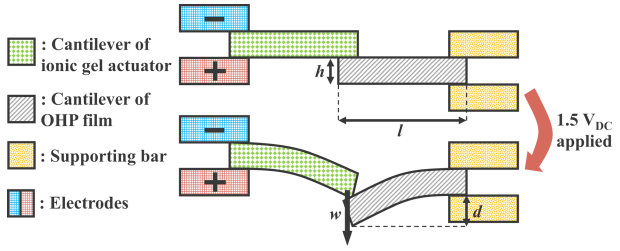

Fig. 9. Measurement principle of the gripping force of the SWIG actuator. The actuator pushes the OHP film cantilever.

TABLE IV
PARAMETERS OF THE OHP FILM CANTILEVER USED IN (3), (4) FOR ESTIMATION OF THE GRIPPING FORCE

Parameters	Values
d (mm)	0.125
l (mm)	8
E (GPa)	0.52
h (μm)	100
b (mm)	2
I (mm^{-4})	1.67×10^{-4}

where d, w, l, E, and I are the displacement, concentrated load at the free end, free length, Young's modulus (longitudinal elastic modulus), and moment of inertia of the OHP cantilever, respectively. Based on Fig. 9, because the concentrated load at the free end w was the same as the force F generated by the ionic gel, we could find the value of F by evaluating w with (3).

The OHP film was cut into 2 mm × 10 mm × 100 μm rectangular pieces to be used as the cantilever for the measurement. A section of the cantilever sized 2 mm × 2 mm was fixed in the jig as shown in Fig. 9. Because the inertia of the film was determined by the 2 mm × 100 μm rectangle, the moment of inertia I was calculated using (4).

$$I = \frac{bh^3}{12} \tag{4}$$

The values of the parameters in (3), (4) are provided in Table IV. The Young's modulus E was acquired using the equation of the strain with another OHP cantilever of 2 mm × 90 mm × 100 μm rectangular form, when a uniformly distributed load was applied (5), by setting the film cantilever parallel to the ground and deforming itself under its own weight,

$$d' = \frac{w' l'^4}{8EI} \tag{5}$$

where d', w', and l' are the displacement, weight, and free length, respectively, of the film cantilever. These values of OHP film are shown in Table V.

The calculation using the values in Table IV and (3)-(5) enabled the generated force F to be obtained as 63.3 μN.

2) Estimation of Young's Modulus of the Sandwich Ionic Gel Actuator: The estimation method for the Young's modulus of the SWIG was the same as that for the OHP film, with the formula for the deformation of the cantilever (4) and (5). The SWIG cantilever of 1.5 mm × 19 mm × 100 μm rectangular form with its 2 mm × 2 mm part fixed in the jig was set parallel to the ground and bending under its own weight. The moment of inertia I and Young's modulus E were estimated with the formula (4) and (5), respectively, under a uniformly distributed load. The values used in the equations are shown in Table V. Consequently, the Young's modulus of the SWIG was estimated as 0.3 MPa. The small Young's modulus of the SWIG compared to 0.52 GPa of the OHP film was supposed to be due to the gel and flexible AgNW electrodes. It contributed to the large deformation of the SWIG actuator at the low operating voltage of 1.5 V_{DC}.

TABLE V
PARAMETERS OF THE CANTILEVER OF THE SWIG AND OHP FILM USED IN (4) AND (5) FOR ESTIMATION OF THE YOUNG'S MODULUS

	OHP	SWIG
d' (mm)	24	8
w' (mg)	143	3
l' (mm)	90	17
b (mm)	2	1.5
h (mm)	0.125	0.1
I (mm^{-4})	8.3×10^{-4}	1.25×10^{-4}
E (Pa)	0.52 G	0.3 M

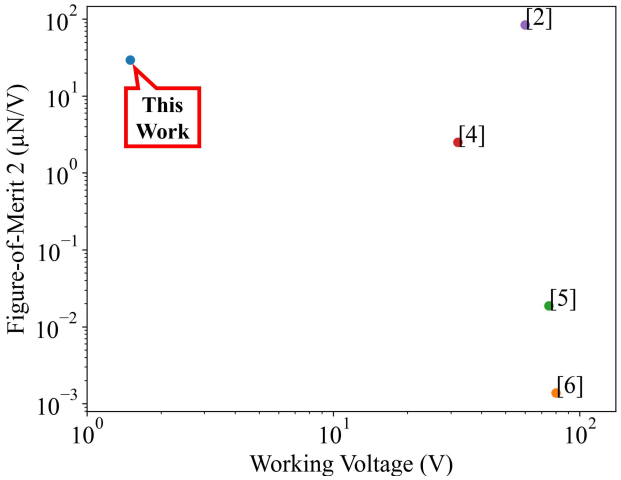

Fig. 10. Figure-of-merit 2 (FoM_2) and working voltage.

G. Comparison of Gripping Performance With That of MEMS Tweezers

To confirm that the tweezer composed of our ionic gel had characteristics appropriate for gripping, the tweezer was compared with existing MEMS tweezers in terms of its gripping force and electrical characteristics. The targets were tweezers driven by voltage or current or composed of IPMC actuators. To enable a fair comparison, suitable figures-of-merit (FoMs) were defined for each of the tweezers and employed as norms.

1) Evaluation With Voltage-Driven MEMS Tweezers: The performance of our ionic gel tweezer is compared with that of comb-drive and piezoelectric tweezers [2], [4]–[6], as given in Table VI and Fig. 10. The comb-drive and piezoelectric actuators operate owing to electrostatic and piezoelectric effects, respectively, generated by the applied voltage. The FoM, FoM_2, is defined as the gripping force normalized by

TABLE VI
PERFORMANCE COMPARISON WITH VOLTAGE-OPERATING TWEEZER

Ref.	How to work	F (μN)	V_{DC} (V)	FoM_2: $F/V_{DC} \times x/a$ (μN/V),	Gripping Target
This Work	IPMCs (SWIG)	**63.3**	**1.5**	**29.5**	**Beads → Organism**
[6]	Comb-drive	**8.7**	80	1.38×10^{-3}	**Pollen**
[5]	Comb-drive	**350**	75	1.88×10^{-2}	**Polystyrene sphere**
[4]	Piezo-electric	15 000	32	2.5	Polystyrene sphere
[2]	Piezo-electric	203 000	60	**84.6**	Nail

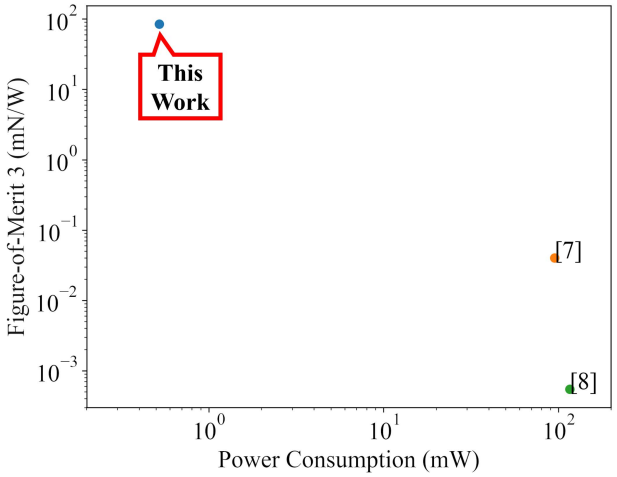

Fig. 11. Figure-of-merit 3 (FoM_3) and power consumption.

the working voltage and maximum displacement at the tip of the actuator, and the expression for this is given in (6).

$$FoM_2 = \frac{F}{V_{DC}} \times \frac{x}{a} \tag{6}$$

where F, V_{DC}, x, and a are the gripping force, DC working voltage, maximum strain at the tip, and total length of the tweezer, respectively. As shown in Fig. 10, our tweezer has a large FoM_2 at the lowest working voltage.

2) Evaluation With Current-Driven MEMS Tweezers: The subjects that were compared were tweezers composed of electrothermal actuators [7], [8] (Table VII). The figure-of-merit FoM_3 is FoM_2 in Subsubsection III-G.1 and is based on the maximum power consumption P instead of V_{DC} (6). This is because the electrothermal actuators deform as a result of joule heat, which was supposed to be the main power consumption of the devices. FoM_3 is expressed as follows:

$$FoM_3 = \frac{F}{P} \times \frac{d}{L} \tag{7}$$

As shown in Fig. 11, our tweezer yielded the maximum FoM_3 for the lowest power consumption.

3) Evaluation With IPMCs Tweezers: Finally, in Table VIII we compared our ionic gel tweezer with tweezers based on IPMC actuators [9]–[12]. All the previous IPMC tweezers contained Nafion as the polymer, whereas the polymer in our actuator was PVDF-TrFE in the SWIG structure. The figure-of-merit, FoM_4, is defined as follows:

$$FoM_4 = F \times FoM_1 \tag{8}$$

where F is the gripping force of the actuator and FoM_1 is the same variable as in (2). We focused on the group of tweezers designed to grip either organisms or tender targets, with single-digit values for FoM_4 in Fig. 12 because our tweezer is designed to grasp vulnerable materials in addition to hard ones gently. As shown in Fig. 12, our tweezer proved to have the highest FoM_4 at the lowest working voltage among the grippers intended to grasp soft materials.

4) Verification of the Gripping Force of the Ionic Gel Tweezer: To confirm that the estimated gripping force 63.3 μN was appropriate for grasping objects softly, we re-examined the generated force and gripping targets in Fig. 10–12 and Table VI–VIII. The gripping force of the tweezers with a non-living rigid substance was almost four or five

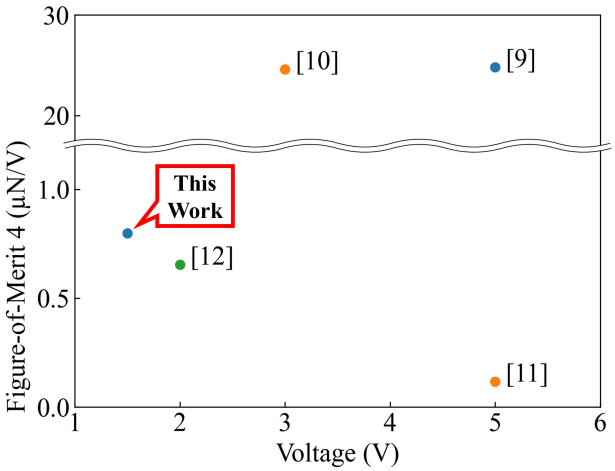

Fig. 12. Figure-of-merit 4 (FoM_4) and working voltage.

TABLE VII
PERFORMANCE COMPARISON WITH CURRENT-OPERATED TWEEZERS

Ref.	How to work	F (μN)	P (m W)	FoM_3: $F/P \times d/L$ (mN/W)	Gripping Target
This Work	IPMCs (SWIG)	**63.3**	**0.52**	**85.2**	**Beads → Organism**
[7]	Electro-thermal	**242**	95	4.00×10^{-2}	**Blood vessel, cell**
[8]	Electro-thermal	0.77	116	5.45×10^{-4}	Glass sphere

TABLE VIII
PERFORMANCE COMPARISON WITH IPMC TWEEZERS

Ref. (IPMCs)	Polymer	F (μN)	V_{DC} (V)	FoM_4: $F \times FoM_1$ (μN/V)	Gripping Target
This Work (SWIG)	PVDF-TrFE	**63.3**	**1.5**	**0.79**	**Beads → Organism**
[11]	Nafion	**170**	5	0.12	**Fish egg**
[12]	Nafion	**85**	2	0.65	**Solder sphere, hydrogel**
[9]	Nafion	18 600	5	24.8	Nuts, Ping-pong ball
[10]	Nafion	10 000	3	24.6	Micropin

orders of magnitude of μN [2], [4], [9], [10]. Meanwhile, those that grasped organisms (pollen [6], blood vessels [7], fish eggs [11]), soft material (hydrogel [12], polystyrene sphere [5]) or even hard objects (solder sphere [12]) had a gripping force of no more than two orders of μN. The calculated force of our tweezer based on 50b SWIG was 63.3 μN of two orders. Therefore, our device with high FoMs had an appropriate force for minimally invasive gripping to gently enclose the various targets.

IV. Conclusion

We realized a self-deformable flexible tweezer capable of gently gripping mm-scale targets and detecting their electrical signals. The self-deformable cantilever in the device was fabricated based on a PVDF-TrFE/EMIMTFSI ionic gel actuator with an electrode consisting of AgNWs using acetone as the solvent. We established a highly reliable manufacturing method with an 89 % yield. Our ionic gel actuator, which contained EMIMTFSI in a weight ratio of 50 wt%, produced the largest displacement of 7 mm for 88 % of the total length of the actuator and the minimum curvature radius of 2 mm at the operating voltage of 1.5 V_{DC}. The flexible cantilever in the tweezer composed of the actuator was proven to detect a sinusoidal signal of 700 mV, at 1 kHz, by deforming itself, the first such example in the world. Simultaneously, the tweezer could grip and release a 5 mm sphere using a gripping force determined to be 63.3 μN, which is appropriate for gripping organisms softly. In the future, we plan to enhance the durability of the ionic gel actuator by improving the electrodes, develop a microfabrication process to separate the electrodes intended for detection from those intended for actuator operation, and demonstrate the gripping of and detection of electrical signals generated by real organisms.

Acknowledgment

The device was fabricated in the MEXT Nanotechnology Platform at the Takeda Sentanchi Supercleanroom. The authors would like to thank Editage (www.editage.com) for English language editing.

References

[1] T. Yamaguchi *et al.*, "Self-deformable flexible MEMS tweezer made of poly (vinylidene fluoride)/ionic liquid gel with electrical measurement capability," in *Proc. 21st Int. Conf. Solid-State Sensors, Actuators Microsyst. (TRANSDUCERS)*, Jun. 2021, pp. 18–21.

[2] R. K. Jain, S. Majumder, and B. Ghosh, "Design and analysis of piezoelectric actuator for micro gripper," *Int. J. Mech. Mater. Des.*, vol. 11, no. 3, pp. 253–276, Sep. 2015.

[3] D. Jaiswal, N. Cowley, Z. Bian, G. Zheng, K. P. Claffey, and K. Hoshino, "Stiffness analysis of 3D spheroids using microtweezers," *PLoS ONE*, vol. 12, no. 11, pp. 1–21, Nov. 2017.

[4] M. Rakotondrabe and I. A. Ivan, "Development and force/position control of a new hybrid thermo-piezoelectric microgripper dedicated to micromanipulation tasks," *IEEE Trans. Autom. Sci. Eng.*, vol. 8, no. 4, pp. 824–834, Oct. 2011.

[5] T. Chen, L. Chen, L. Sun, and X. Li, "Design and fabrication of a four-arm-structure MEMS gripper," *IEEE Trans. Ind. Electron.*, vol. 56, no. 4, pp. 996–1004, Apr. 2009.

[6] B. Piriyanont and S. O. R. Moheimani, "MEMS rotary microgripper with integrated electrothermal force sensor," *J. Microelectromech. Syst.*, vol. 23, no. 6, pp. 1249–1251, Dec. 2014.

[7] R. Zhang, J. Chu, H. Wang, and Z. Chen, "A multipurpose electrothermal microgripper for biological micro-manipulation," *Microsyst. Technol.*, vol. 19, no. 1, pp. 89–97, Jan. 2013.

[8] T. C. Duc, G. K. Lau, J. F. Creemer, and P. M. Sarro, "Electrothermal microgripper with large jaw displacement and integrated force sensors," *J. Microelectromech. Syst.*, vol. 17, no. 6, pp. 1546–1555, Dec. 2008.

[9] Q. He *et al.*, "The highly stable air-operating ionic polymer metal composite actuator with consecutive channels and its potential application in soft gripper," *Smart Mater. Struct.*, vol. 29, no. 4, Mar. 2020, Art. no. 045013.

[10] R. Jain, S. Datta, S. Majumder, and A. Dutta, "Two IPMC fingers based micro gripper for handling," *Int. J. Adv. Robot. Syst.*, vol. 8, no. 1, pp. 1–9, Mar. 2011.

[11] H. R. Cheong, C. Y. Teo, P. L. Leow, K. C. Lai, and P. S. Chee, "Wireless-powered electroactive soft microgripper," *Smart Mater. Struct.*, vol. 27, no. 5, Apr. 2018, Art. no. 055014.

[12] R. Lumia and M. Shahinpoor, "IPMC microgripper research and development," *J. Phys., Conf. Ser.*, vol. 127, Aug. 2008, Art. no. 012002.

[13] Y. T. Tang, J. Kim, H. E. López-Valdés, K. C. Brennan, and Y. S. Ju, "Development and characterization of a microfluidic chamber incorporating fluid ports with active suction for localized chemical stimulation of brain slices," *Lab Chip*, vol. 11, no. 13, pp. 2247–2254, Jul. 2011.

[14] A. Jonsson *et al.*, "Bioelectronic neural pixel: Chemical stimulation and electrical sensing at the same site," *Proc. Nat. Acad. Sci. USA*, vol. 113, no. 34, pp. 9440–9445, Aug. 2016.

[15] R. Mejri, J. C. Dias, S. B. Hentati, M. S. Martins, C. M. Costa, and S. Lanceros-Mendez, "Effect of anion type in the performance of ionic liquid/poly(vinylidene fluoride) electromechanical actuators," *J. Non-Crystalline Solids*, vol. 453, pp. 8–15, Dec. 2016.

[16] S. Imaizumi, H. Kokubo, and M. Watanabe, "Polymer actuators using ion-gel electrolytes prepared by self-assembly of ABA-Triblock copolymers," *Macromolecules*, vol. 45, no. 1, pp. 406–407, Dec. 2012.

[17] K. Hata, T. Inoue, and M. Katayama, "Proposal for the operation model of ionic polymer actuators including saturated ionic liquid," *Trans. Soc. Instrum. Control Eng.*, vol. 53, no. 1, pp. 73–79, Jan. 2017.

[18] N. Terasawa *et al.*, "Effect of hexafluoropropylene on the performance of poly(vinylidene fluoride) polymer actuators based on single-walled carbon nanotube–ionic liquid gel," *Sens. Actuators B, Chem.*, vol. 160, no. 1, pp. 161–167, Dec. 2011.

[19] T. Fukushima, K. Asaka, A. Kosaka, and T. Aida, "Fully plastic actuator through layer-by-layer casting with ionic-liquid-based Bucky gel," *Angew. Chem. Int. Ed.*, vol. 44, no. 16, pp. 2410–2413, Apr. 2005.

[20] T. Sugino, K. Kiyohara, I. Takeuchi, K. Mukai, and K. Asaka, "Actuator properties of the complexes composed by carbon nanotube and ionic liquid: The effects of additives," *Sens. Actuators B, Chem.*, vol. 141, no. 1, pp. 179–186, Aug. 2009.

[21] J. C. Dias *et al.*, "Improved response of ionic liquid-based bending actuators by tailored interaction with the polar fluorinated polymer matrix," *Electrochim. Acta*, vol. 296, pp. 598–607, Feb. 2019.

[22] Y. Liu, M. Ghaffari, R. Zhao, J.-H. Lin, M. Lin, and Q. M. Zhang, "Enhanced electromechanical response of ionic polymer actuators by improving mechanical coupling between ions and polymer matrix," *Macromolecules*, vol. 45, no. 12, pp. 5128–5133, Jun. 2012.

[23] Q. Pei and O. Inganaes, "Electrochemical applications of the bending beam method. 1. Mass transport and volume changes, in polypyrrole during redox," *J. Phys. Chem.*, vol. 25, no. 96, pp. 10507–10514, Dec. 1992.

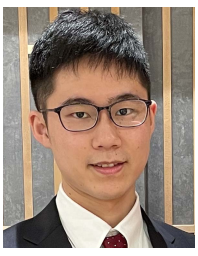

Takafumi Yamaguchi (Graduate Student Member, IEEE) was born in Yokohama, Japan, in 1998. He received the B.E. degree in electrical engineering from The University of Tokyo, Tokyo, Japan, in 2021, where he is currently pursuing the M.E. degree. His research interest is flexible MEMS device by integration of ionic gel actuator.

Naoto Usami (Member, IEEE) received the B.E., M.E., and Ph.D. degrees in electrical engineering from The University of Tokyo in 2014, 2016, and 2019, respectively. In 2014, he has served as a Project Manager for the realization of deep space sculpture "DESPATCH" which was a part of the ARTSAT Project. Since 2021, he has been an Assistant Professor of the Institute of Space and Astronautical Science (ISAS), Japan Aerospace Exploration Agency (JAXA). His current interests include robotic and wireless system for planetary exploration, micro- and nano-fabrication, and reconfigurable autonomous distributed microsystems.

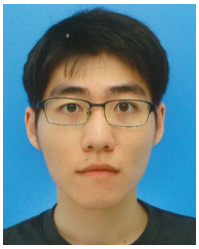

Kei Misumi (Graduate Student Member, IEEE) was born in Santiago de Chile, Chile, in 1998. He received the B.S. and M.S. degrees in electronical engineering from The University of Tokyo, Tokyo, Japan, in 2020 and 2022, respectively, where he is currently pursuing the Ph.D. degree with the Department of Electrical Engineering and Information Systems. His focus is on microfabrication and integration of MEMS and intelligent systems.

Atsushi Toyokura received the B.Sc. degree from the Department of Computer Science, Chiba Institute of Technology, Chiba. He is currently a Technical Specialist at the Department of Electrical Engineering, The University of Tokyo, Tokyo. His research interests are material processing, electronic circuit, and embedded software.

Akio Higo (Member, IEEE) received the B.E. degree from Seikei University, Tokyo, Japan, in 2002, and the M.E. and Ph.D. degrees from the Department of Electrical Engineering, The University of Tokyo, Tokyo, in 2004 and 2007, respectively. From 2007 to 2012, he was an Assistant Professor with the Research Center for Advanced Science and Technology. From 2012 to 2016, he was an Assistant Professor with the World Premier Initiative Advanced Institute for Materials Research, Tohoku University, Sendai, Japan. Since 2017, he has been a Project Lecturer with the D2T Research Division, VLSI Design and Education Center, and currently with the Systems Design Laboratory, D2T Research Department, School of Engineering, The University of Tokyo. His research interests include NEMS/MEMS, nanolithography for III–V materials and silicon, and silicon photonics.

Shimpei Ono was born in Japan, in 1973. He received the Ph.D. degree from the Tokyo Institute of Technology in 2006. He has conducted research at the Central Research Institute of Electric Power Industry as well as the University of Geneva, RIKEN, The University of Tokyo, Kyoto University, and the Tokyo Science University, as a Visiting Scientist. In 2012, he was awarded as the Chair of Excellence in the framework of 'Laboratoire d'Alliances Nanosciences-Energies du Futur' (LANEF) in Grenoble to conduct a project titled "Development of Iontronics."

Gilgueng Hwang (Member, IEEE) was born in Jinju, South Korea, in 1977. He received the B.S. degree in electrical engineering from Yonsei University, Seoul, South Korea, in 2002, and the M.S. and Ph.D. degrees in electrical engineering from The University of Tokyo, Tokyo, Japan, in 2005 and 2008, respectively.

He has spent two years at ETH Zürich, Switzerland, as an Academic Guest for a collaborative research project. Then, he worked as a Post-Doctoral Researcher for two years at ISIR, Sorbonne University, Paris, France. Since 2010, he has been working as a Chargé de Recherche at CNRS-C2N, Paris-Saclay University, Palaiseau, France. He is currently a Visiting Scholar at LIMMS, The University of Tokyo, which is an international joint research laboratory of The University of Tokyo and CNRS. His research interests cover micro/nanorobotics, micro/nanofluidics, lab-on-a-chip, 3-D helical nanobelts, *in-situ* SEM characterization, nanomanipulation, and nanoassembly.

Guilhem Larrieu (Member, IEEE) received the Ph.D. degree in electronics from the University of Lille in 2004. He obtained a Post-Doctoral Fellowship at The University of Texas at Arlington (UTA). In late 2005, he secured an independent researcher position at IEMN-CNRS Laboratory, Lille, on MOS transistor technology. In 2010, he moved to LAAS-CNRS to establish a new research axis on vertical nanowire based-devices. From 2019 to 2021, he was an Invited Researcher at The University of Tokyo to extend its nanoelectrode concepts to interface with high resolution human organoids. His laboratory is composed of three post-doctoral researchers and six Ph.D. students and supported by several technical staff members. He is currently the Director of research at CNRS, working at LAAS-CNRS Laboratory, Toulouse, France, and a Research Fellow at the Institute of Industrial Science, The University of Tokyo, Japan. He is leading an activity on nano-&neuro-electronics aiming at developing new devices based on functional nanostructures for ultimate nanoelectronics and for innovative biosensor platforms in particular for neural interfacing. These activities are articulated around nanotechnologies, nanodevice, nanoelectronics, cell cultures, and electrophysiology. He has regularly participated in or coordinated research proposals in response to local, national, or European calls for projects (in particular eight European projects). Overall, he has supervised 14 Ph.D. students and eight post-doctoral researchers which now either obtained academia positions (an Assistant Professor at Aix-Marseille University and the University of Toulouse) or in the semiconductor industry (Huawei, STMicro, XFAB, Tronics, and Aledia). He is the author/coauthor of over 70 articles in peer-reviewed international journals, 13 patents as a principal investigator, and more than 30 invited contributions to conferences.

Yoshiho Ikeuchi received the Ph.D. degree from The University of Tokyo in 2007. He received post-doctoral neuroscience training at the Harvard Medical School from 2007 to 2013 and Washington University, St. Louis, from 2013 to 2014. He was appointed as a Lecturer in 2014 and then an Associate Professor in 2018 at the Institute of Industrial Science, The University of Tokyo. His goal of research is to create nervous tissue (organoids) from human multipotent stem cells (iPS cells) and to functionalize them in order to better understand the mechanisms of the brain. His group has successfully developed technology to connect neural organoids via an axon bundle which mimic neuronal circuits in the human body.

Agnés Tixier-Mita (Member, IEEE) was born in Bourg-la-Reine, France, in 1970. She received the B.S. and M.S. degrees in material sciences from the ÉNSI de Caen, University of Caen Normandy, France, in 1994, and the Ph.D. degree from the University of Lille I, France, in 1998.

She then joined the LIMMS-CNRS/IIS, The University of Tokyo, in 1999, as a Post-Doctoral Fellow Researcher for two years. Then, she joined the Institute of Industrial Sciences, The University of Tokyo, as an Assistant Researcher. She has been affiliated to RCAST and IIS, The University of Tokyo, from 2010 to 2020, as an Associate Professor, and then to IIS since 2020. Her research interests include integrated sensor-array devices for biological applications based on CMOS and thin-film-transistor technologies. She is a member of IEEJ.

Ken Saito (Member, IEEE) was born in Tokyo, Japan, in 1978. He received the B.S. and M.S. degrees in electronic engineering and the Ph.D. degree in engineering from Nihon University, Tokyo, in 2001, 2004, and 2010, respectively.

He was a Research Assistant at the Department of Physics, College of Humanities and Sciences, Nihon University, from 2007 to 2010; a Research Assistant at the Department of Precision Machinery Engineering, College of Science and Technology, Nihon University, from 2010 to 2011; an Assistant Professor at Nihon University from 2011 to 2017; and an Associate Professor at Nihon University from 2017 to 2021. He was also a Visiting Scholar at the University of California, Berkeley. He is currently a Professor at the Department of Precision Machinery Engineering, College of Science and Technology, Nihon University, Funabashi-shi, Chiba, Japan. His current research interests include hardware neural networks and microrobots. He is a member of INNS, IEEJ, IEICE, *JSME*, and *JIEP*.

Timothée Lévi (Member, IEEE) received the Ph.D. degree in electronics from the University of Bordeaux, France, in 2007. Since October 2009, he has been an Associate Professor at the IMS Laboratory, University of Bordeaux. During this period, from September 2013 to August 2015, he was a Visiting Research Fellow at The University of Tokyo, Japan. From 2017 to 2020, he was a Project Associate Professor at The University of Tokyo. His research interest deals with neuromorphic engineering which aims at designing and using integrated circuits which components and architecture are neuro-mimetic for bio-hybrid experiments.

Yoshio Mita (Senior Member, IEEE) received the B.E., M.E., and Ph.D. degrees from the Department of Electrical and Electronic Engineering, The University of Tokyo (UTokyo), Japan, 1995, 1997, and 2000, respectively. Since 2000, he has continuously been working as a Faculty Member of the Graduate School of Engineering, UTokyo. He has been a Co-Principal Investigator (PI) of the Intelligent Semiconductor Microdevices Laboratory (iSML) since 2002 and a single PI since 2013. He is currently a Professor of the Department of Electrical Engineering and Information Systems, Graduate School of Engineering, UTokyo. He is also the Leader of UTokyo's open nanofabrication platform supercleanroom activity (aka. Takeda Semtanchi SCR). He has published 71 journal articles and 151 reviewed international conference papers, including four keynote and 14 invited talks. His research interests include CMOS and MEMS integration technology and its applications, such as a high voltage photovoltaic for autonomous distributed micro systems.